Molecular gas in the elliptical galaxy NGC 759

Interferometric CO observations

T. Wiklind[1], **F. Combes**[2], **C. Henkel**[3], **F. Wyrowski**[3,4]

[1] Onsala Space Observatory, S–43992 Onsala, Sweden
[2] DEMIRM Observatoire de Paris, 61 Avenue de l'Observatoire, F–75014 Paris, France
[3] Max-Planck-Institut für Radioastronomie, Auf dem Hügel 69, D–53121 Bonn, Germany
[4] Physikalisches Institut der Universität zu Köln, Zülpicher Strasse 77, D–50937 Köln, Germany

Abstract. We present interferometric observations of CO(1–0) emission in the elliptical galaxy NGC 759 with an angular resolution of $3''1 \times 2''3$ (990×735 pc at a distance of 66 Mpc). NGC 759 contains $2.4 \times 10^9 \, M_\odot$ of molecular gas. Most of the gas is confined to a small circumnuclear ring with a radius of 650 pc with an inclination of 40°. The maximum gas surface density in the ring is $750 \, M_\odot \, pc^{-2}$. Although this value is very high, it is always less than or comparable to the critical gas surface density for large scale gravitational instabilities. The CO $J=2-1/J=1-0$ line ratio is low (0.4), implying sub-thermal excitation. This low ratio is consistent with a two–component molecular gas, consisting of a cold and dense phase, containing most of the mass, and a warm and diffuse gas component, dominating the CO emission. Compared to galaxies of similar gas surface densities, NGC 759 is underluminous in $L_{\rm FIR}$ with respect to its molecular gas mass, suggesting that the star forming efficiency in NGC 759 is low. We discuss the possibility that the molecular gas and current star formation activity in NGC 759 could be signatures of a late stage of a merging between two gas–rich disk galaxies. We use a mass model of the underlying galaxy which is applicable to spherical galaxies with an $r^{1/4}$–luminosity profile when interpreting our CO data. This leads to more modest estimates of the molecular gas mass fraction and the surface gas density than would have been derived using simpler models, suggesting that many of the spectacular molecular gas properties of ultraluminous FIR galaxies, which could be described by similar mass distributions, may have to be revised.

Key words: ISM: molecules – Galaxies: elliptical and lenticular, cD – Galaxies: individual: NGC759 – Galaxies: ISM – Galaxies: kinematics and dynamics

1. Introduction

Faber & Gallagher (1976) found the apparent absence of an interstellar medium (ISM) in elliptical galaxies surprising since mass loss from evolved stars should contribute as much as $10^9 - 10^{10} \, M_\odot$ of gas to the ISM during a Hubble time. Today we know that ellipticals do contain an ISM, albeit very different from that found in spiral galaxies. The most massive ISM component is a hot X–ray radiating halo, with a typical mass of $10^8 - 10^{10} \, M_\odot$ (Fabbiano 1990). Small amounts of photoionized gas (typically $10^2 - 10^4 \, M_\odot$) can be found in about 60% of all ellipticals (Caldwell 1984, Phillips et al. 1986). In addition, $\sim 45\%$ of a magnitude limited sample of ellipticals were detected at both 60 and $100 \, \mu$m by IRAS (Jura et al. 1987, Knapp et al. 1989), suggesting the presence of a significant dust component. Atomic hydrogen gas is seen in $\sim 15\%$ of all ellipticals (Knapp et al. 1985). A similar detection rate has been found for molecular gas, seen through CO emission (Lees et al. 1991, Wiklind et al. 1995).

Elliptical galaxies have less molecular gas per blue luminosity than spirals and a much larger dispersion in their $L_{\rm B}/M_{\rm H_2}$ ratios. Wiklind et al. (1995) found that the molecular gas in ellipticals is *not* correlated with the old stellar population and, hence, is accreted from an external source. A similar result for the atomic hydrogen gas was reached by Knapp et al. (1985).

The discovery of kinematically decoupled cores in elliptical galaxies has strongly favoured the idea that these systems can be formed through the merging of two disk galaxies of similar sizes (Franx & Illingworth 1988, Rix & White 1992). The main stellar component is hot and slowly rotating while a small centrally concentrated and kinematically distinct core exhibits rapid rotation. Numerical simulations of mergers between two disk galaxies suc-

cessfully reproduce the observed properties (Hernquist & Barnes 1991). The dissipative gas is concentrated in the center of the resulting galaxy and the kinematically decoupled core is observable in both ionized and molecular gas (cf. Bertola & Bettoni 1988, Balcells & Stanford 1990, Wang et al. 1992). The early stages of mergers are accompanied by intense and efficient star formation, giving a chaotic appearance to the system. The underlying old stellar population, however, has a luminosity profile which in most cases closely follows the de Vaucouleurs $r^{1/4}$ law. Hence, once the gas has been consumed and star formation ceases, the resulting system will not only resemble but actually be an elliptical galaxy.

One elliptical with relatively strong CO emission is NGC 759 (Wiklind et al. 1995). We have chosen this galaxy for high resolution observations with the aim of resolving the distribution and kinematical structure of the molecular gas. In this paper we present our results and discuss the rather peculiar conditions under which the molecular gas exists in this galaxy.

2. Abell 262 and NGC 759

NGC 759, a giant E0 galaxy, is one of the brightest members of the cluster A262 and forms a noninteracting pair with NGC 753. The cluster A262 is comparable to the Virgo cluster in its richness and has a similar X–ray luminosity. The X–ray emission is centered on the elliptical NGC 708, which appears to be at rest within the cluster (Jones & Forman 1984). NGC 708 is a radio source with a dust lane oriented almost perpendicular to its radio axis (Ebneter & Balick 1985). Its far–infrared (FIR) luminosity derived from IRAS data is $3 \times 10^9 \, \mathrm{L_\odot}$. A deep search for CO emission in NGC 708 gave an upper limit to the molecular gas mass of $4 \times 10^7 \, \mathrm{M_\odot}$ (Braine & Dupraz 1994).

An optical spectroscopic survey of ten early–type galaxies in A262 (including NGC 708 and NGC 759) showed that only NGC 759 has a spectrum showing recent star formation activity (Vigroux et al. 1989). A recent study of NGC 759 (E. Davoust private communication) shows emission lines of $H\alpha$, NII and SII. The FIR luminosity of NGC 759 is $1.1 \times 10^{10} \, \mathrm{L_\odot}$ and we observe a CO luminosity corresponding to an H_2 mass of $2.4 \times 10^9 \, \mathrm{M_\odot}$ (Wiklind et al. 1995; Table 1). Despite the presence of a massive cold ISM component, NGC 759 is a true giant elliptical: It has an $r^{1/4}$ light profile (i.e. Sandage & Perelmuter 1991) and it falls upon the fundamental plane relationship for elliptical galaxies (c.f. Djorgovski & Davis 1987; Guzmán et al. 1993).

3. Observations and data reduction

3.1. Observations

Synthesis observations of NGC 759 were made with the Institute de Radio Astronomie Millimètrique (IRAM) interferometer at Plateau de Bure (PdB), situated at an

Table 1. Data on NGC 759

Type	E0 (E1)		(1)
Size	$1'.6 \times 1'.4$		(1)
R.A. (2000)	$01^\mathrm{h}57^\mathrm{m}50.3^\mathrm{s}$		(2)
DEC (2000)	$+36°20'35''$		(2)
$V_\odot$	4665	$\mathrm{km\,s^{-1}}$	(3,4)
Distance$^{a)}$	66	Mpc	(3)
R_{25}	14.5	kpc	(4)
B_T^0	13.24		(1)
M_B	-20.86		(3)
$(B-V)_\mathrm{T}^0$	1.00		(1)
$(U-B)_\mathrm{T}^0$	0.52		(1)
S_{12}	< 102	mJy	(5)
S_{25}	< 132	mJy	(5)
S_{60}	732 ± 66	mJy	(5)
S_{100}	2076 ± 187	mJy	(5)
$S_{1.4GHz}$	16.4	mJy	(6)
L_B	3.46×10^{10}	$\mathrm{L_\odot}$	(4)
L_FIR	1.13×10^{10}	$\mathrm{L_\odot}$	(4)
L_CO	5.03×10^8	$\mathrm{K\,km\,s^{-1}\,kpc^{-2}}$	(4)
M_{H_2}	2.4×10^9	$\mathrm{M_\odot}$	(4)
M_HI	$< 7.4 \times 10^8$	$\mathrm{M_\odot}$	(7)
M_d	3.5×10^6	$\mathrm{M_\odot}$	(4)
$T_\mathrm{d}{}^{b)}$	31	K	(4)
SFR$^{c)}$	7	$\mathrm{M_\odot\,yr^{-1}}$	(3)
$L_\mathrm{FIR}/M_{\mathrm{H}_2}$	4.7	$\mathrm{L_\odot/M_\odot}$	(4)
$L_\mathrm{FIR}/L_\mathrm{B}$	0.3	$\mathrm{L_\odot/L_{BOL}}$	(4)

(1) RC3 (de Vaucouleurs et al. 1991).
(2) Peak of the CO and radio continuum emission (cf. Fig. 2).
(3) Adopted in this paper.
(4) Wiklind et al. (1995).
(5) IRAS Faint Source Catalog.
(6) Feretti & Giovannini (1994).
(7) Huchtmeier et al. (1995).

a) Derived from the mean heliocentric velocity of the A262 cluster 4845 ± 438 (Moss & Dickens 1977) and a Hubble constant of $75 \, \mathrm{km\,s^{-1}\,Mpc^{-1}}$, corrected for the solar motion relative to the Local Group and the peculiar motion of the Local Group with respect to the Virgo cluster (Aaronson et al. 1982).
b) Derived using a ν^1 emissivity law. The dust temperature is slightly lower than in ref (4) due to modified FIR fluxes.
c) Derived using $SFR \approx 6.5 \times 10^{-10} \, L_\mathrm{FIR} \, \mathrm{M_\odot \, yr^{-1}}$.

altitude of 2560 m. The PdB array comprises 4 telescopes of 15–m diameter which can be placed at 26 different stations along a T–shaped runway extending 288 m East–West and 160 m North–South (for a detailed description, see Guilloteau et al. 1992). NGC 759 was observed with the standard CD configuration (see Table 2). Maximum and minimum baselines were 160 and 24 m, respectively. The observations were made on 7 occasions between June 1993 and March 1994, with a total observing time of 52.5 hours. The SIS receivers were single–sideband tuned to the redshifted ^{12}CO, $J=1-0$ frequency 113.508 GHz, with the CO line placed in the upper sideband. The receiver temperatures were 40–140 K, resulting in system temperatures of 300–800 K (T_A^*). The correlator was configured as five slightly overlapping 64×2.5 MHz subbands, giving a ve-
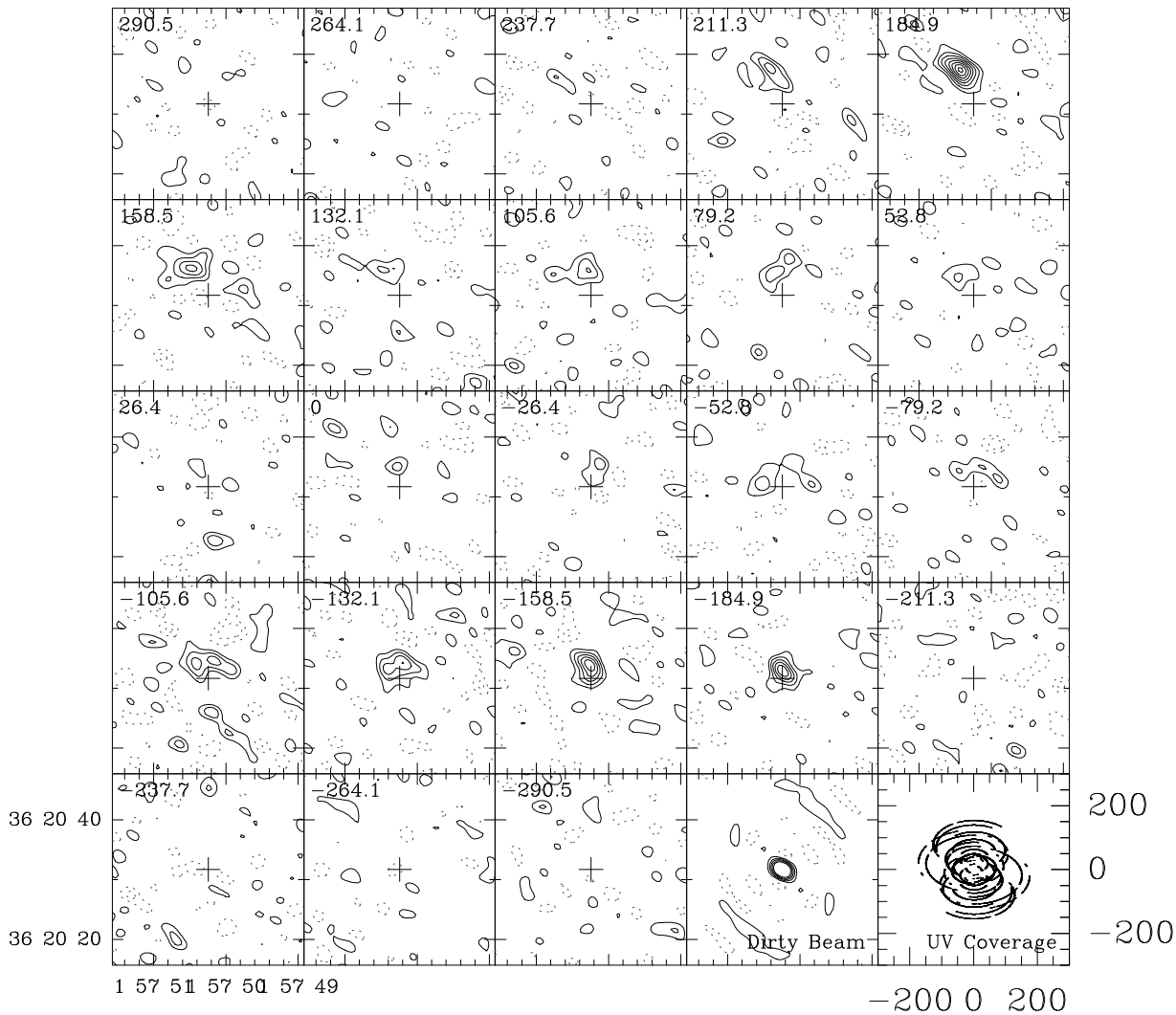
Fig. 1. Channel maps of the CO emission in NGC 759, separated by 10 MHz ($26.4 \, \mathrm{km \, s^{-1}}$). Velocity offsets are relative to the systemic velocity of $4665 \, \mathrm{km \, s^{-1}}$. The cross in each map corresponds to the phase reference center. The contour levels are in steps of 10 mJy (0.13 K). Also shown are the dirty beam and the uv–coverage. The latter is in units of meters. Coordinates are J2000.0.

locity resolution of $6.6 \, \mathrm{km \, s^{-1}}$ and a total bandwidth of $1340 \, \mathrm{km \, s^{-1}}$.

3.2. Data reduction

The CLIC programme and associated Grenoble software were used for all stages of the data reduction. Bad scans were flagged, followed by bandpass calibration using strong continuum sources observed in the beginning of each observing run. Each correlator subband was fitted separately with a 7–10th order polynomial. The edges and two channels in the center of the subband were affected by the Gibbs phenomenon and were omitted in the fitting process. The errors in the amplitude and phases for the

bandpass correlations were $2 - 8\%$ and $1.2 - 4°$, respectively.

Cubic splines were fitted to the measured phases of the phase calibrators. In a few cases a focus measurement during the observations introduced a phase jump. In order to match these discontinuities we applied two fits separately. Due to bad weather conditions the observations in June 27, August 31, and September 3 had residual phase errors of $25 - 35°$. The rest of the observations have residual phase errors of $5 - 15°$.

Long integrations on either 3C345, 3C454.3 or 3C84 were made at the beginning of each observing run. These sources were used as bandpass calibrators as well as flux references. Since most calibrator sources at millimeter
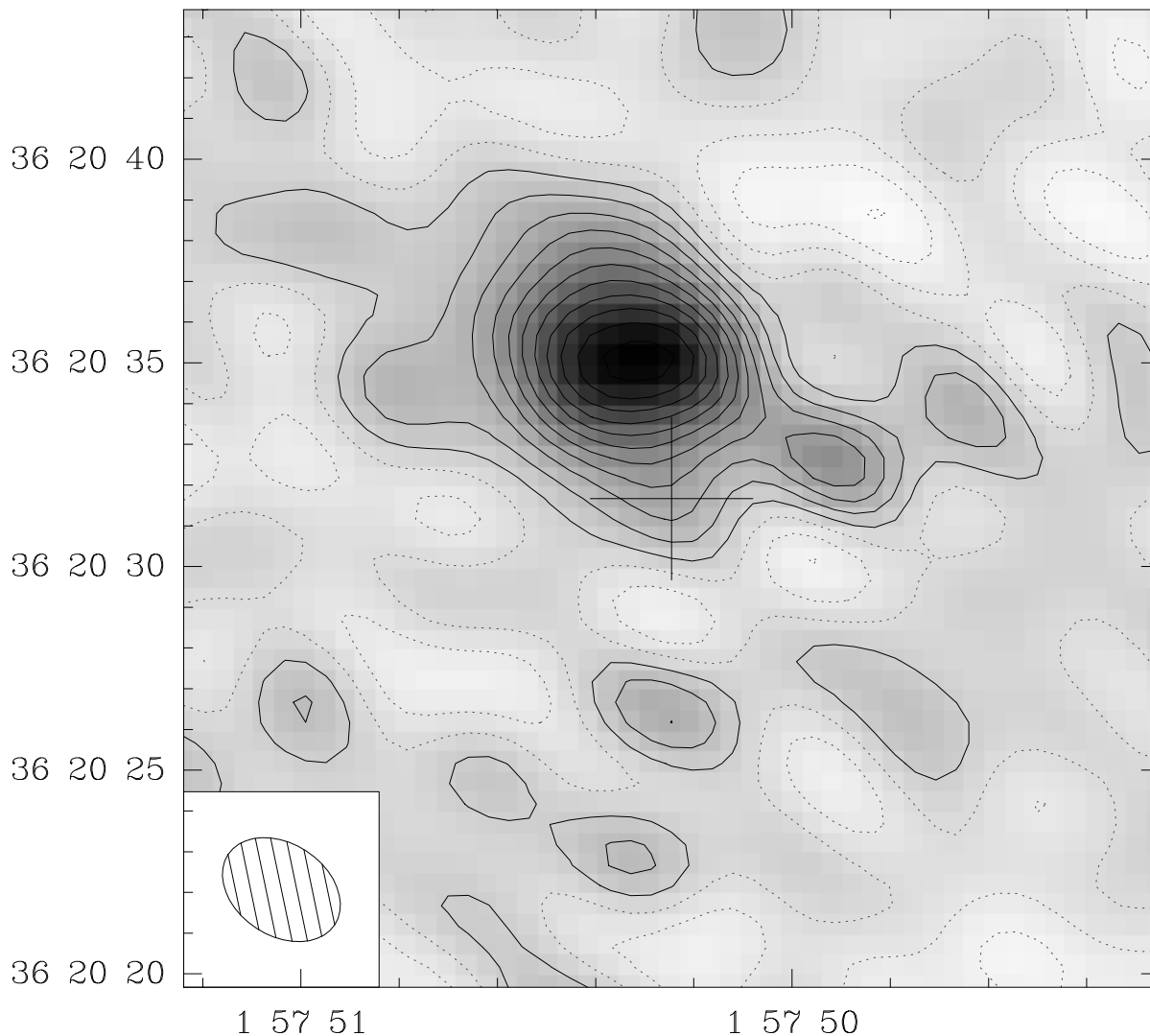
Fig. 2. Total integrated CO(1–0) emission obtained by adding all channels between $-237\,\mathrm{km\,s^{-1}}$ and $+185\,\mathrm{km\,s^{-1}}$ (relative to the systemic velocity). The level spacing is $0.8\,\mathrm{Jy\,km\,s^{-1}}$ and the rms noise in the map is $0.8\,\mathrm{Jy\,km\,s^{-1}}$. The cross marks the phase reference center and the optical position, but is offset a few arcsec from the CO and radio continuum peaks (see text for details). Coordinates are J2000.0.

wavelengths are variable, it is difficult to apply a correct flux scale. The flux values were bootstrapped from measurements of sources with accurately known fluxes. For 3C84 we used $5.1\pm0.8\,\mathrm{Jy}$ and for 3C454.3 $6.9\pm0.8\,\mathrm{Jy}$, derived with the IRAM 30–m telescope in August 1993. We could not get a reasonable solution using $6.2\,\mathrm{Jy}$ for 3C345, derived in February 1993. Instead we used 0235+285, with $2.05\,\mathrm{Jy}$ derived in July 1993. For the March 29 1994 observation 0133+476 was used as a flux calibrator ($1.45\,\mathrm{Jy}$). The adopted fluxes were used to calculate the antenna gains. With these gains the fluxes of all phase calibrators were determined, only using scans with the highest amplitudes to ensure that no phase fluctuations had reduced the

amplitude. Cubic splines were then fitted to the NGC 759 data.

From the calibrated data we constructed uv–tables, applied a fast Fourier transformation and deconvolved the resulting maps with the CLEAN algorithm using natural weighting. The resulting size of the clean beam is $3''.1\times2''.3$, corresponding to $990\times735\,\mathrm{pc}$ at a distance of $66\,\mathrm{Mpc}$. The dirty beam and the uv–coverage are shown as part of Fig. 1.

4. Results

Date	Configuration[a]	Hours	Bandpass calibrator	Phase calibrator
27 June 1993	N05 N13 E10	8.5	3C345	0234+285
1–2 Jul 1993	N05 N13 E10 W12	9.2	3C454.3	0234+285
19–20 Aug 1993	E03 W05 N05	7.4	3C84	3C84
21 Aug 1993	E03 N05 W00	5.0	3C84	3C84
31 Aug – 1 Sep 1993	E10 W09 N15 N03	10.7	3C84	3C84
3–4 Sep 1993	E10 W09 N15 N03	9.6	3C84	3C84
29 Mar 1994	E03 N05 W00 W05	2.2	3C345	0133+476, 3C84

a) N, W and E refer to the northern, western and eastern arm, respectively. Numbers denote the distance from the intersection of the arms (W00) in units of 8 m.

4.1. The CO distribution

Individual channel maps with a velocity separation of $26.4\,\mathrm{km\,s^{-1}}$ (10 MHz) are shown in Fig. 1. CO emission is clearly detected in channels approximately $\pm 200\,\mathrm{km\,s^{-1}}$ around the systemic velocity of $4665\,\mathrm{km\,s^{-1}}$. The strongest emission is seen around $+185$ and $-185\,\mathrm{km\,s^{-1}}$ relative to the systemic velocity, with peak flux densities of 95 and 65 mJy per beam. The rms noise in the individual maps is 6 mJy per beam.

A map of the total integrated CO emission was made by adding all the channels between $-237\,\mathrm{km\,s^{-1}}$ and $+185\,\mathrm{km\,s^{-1}}$. The result is presented in Fig. 2. The peak of the CO emission is $9.2\,\mathrm{Jy\,km\,s^{-1}}$. By summing the same number of channels without emission we obtained an rms noise of $0.8\,\mathrm{Jy\,km\,s^{-1}}$.

Two things are immediately evident from Fig. 2. First of all, the peak of the CO emission is offset $\sim 4''$ from the nominal pointing of the telescope. Since the peak of the CO emission also corresponds to the kinematical center, as well as the center of radio continuum emission (Feretti & Giovannini 1994), this offset most likely reflects an uncertainty in the optical coordinates. Secondly, the emission region has an elliptical shape, with an extent of $5''4 \times 4''3$ (1.8×1.4 kpc) at the 50% level. This is larger than the synthesized beam which has a FWHM size of $3''1 \times 2''3$. However, the synthesized beam and the CO emission region have similar ratios of the major and minor axis as well as the same position angle ($\sim 50°$). This could be a coincidence or an indication that our synthesized beam is larger than estimated. In addition to the bright compact component, there is low level emission extending towards the South–West, to a distance of $\sim 7''$ from the center.

At a frequency of 113.5 GHz and with the CD configuration, the PdB interferometer will not detect emission more extended than about $30''$, corresponding to ~ 10 kpc at a distance of 66 Mpc. We can check if such extended emission exists in NGC 759 by comparing our single dish flux with the flux obtained with the interferometer. Integrating the emission above $0.8\,\mathrm{Jy\,km\,s^{-1}}$ for the interferometer data, we obtain a total flux of $37 \pm 2\,\mathrm{Jy\,km\,s^{-1}}$. The single dish CO(1–0) spectrum obtained with the IRAM 30–m telescope has an integrated flux of $11.8\,\mathrm{K\,km\,s^{-1}}$ (Wiklind et al. 1995). Converting the single dish CO(1–0) flux to Jy using $4.47\,\mathrm{Jy/K}$, we get 53 ± 3 Jy. The interferometer thus recovers $\sim 70\%$ of the single dish flux. It is possible that 30% of the emission seen with the single dish telescope is uniformly extended over more than 10 kpc; however, given the uncertainties associated with calibration (about 30% for both single dish and interferometric data) and the fact that the emission profiles are very similar in shape (see Fig. 3), we believe that it is more likely that almost all molecular gas seen with the single dish telescope is concentrated within the central $5''$.

4.2. The velocity field

The channel maps in Fig. 1 show strong CO emission in channels at approximately $\pm 185\,\mathrm{km\,s^{-1}}$ from the center velocity. These channels correspond to the two peaks in the double–horned profile shown in Fig. 3a. A close inspection of the channel maps shows that the two main emission regions are separated by a few arcseconds. The separation is, however, of the order of the angular resolution. We therefore made Gaussian fits to the individual channels, finding a systematic shift in center velocity with position, with redshifted emission coming from the North–East and blueshifted from the South–West (Fig. 4). From a fit to the velocities in Fig. 4 we derive a position angle of $\sim 50°$, measured from North to East.

A position–velocity diagram along a position angle of $50°$ is shown in Fig. 5, where the offsets in position are relative to the peak of the integrated emission. The two peaks of CO emission seen in Fig. 5 are symmetrical with respect to the center, both in position and velocity. The separation of the two peaks is $4''$, corresponding to 1.3 kpc.
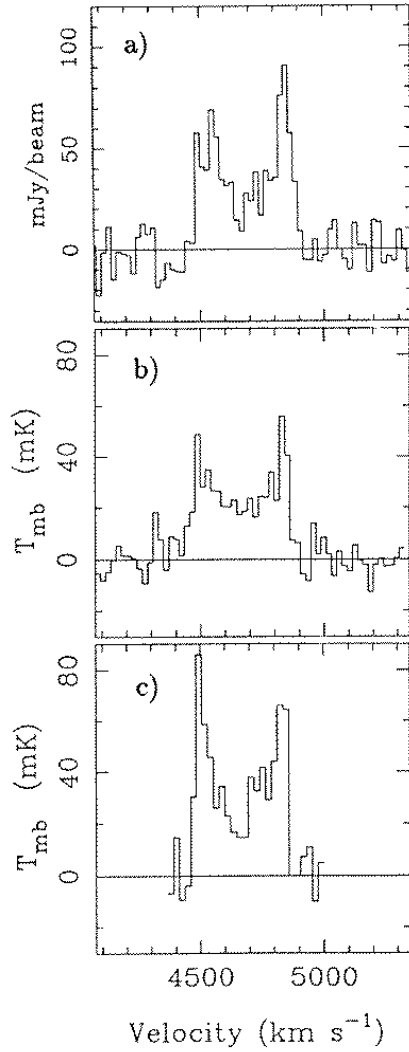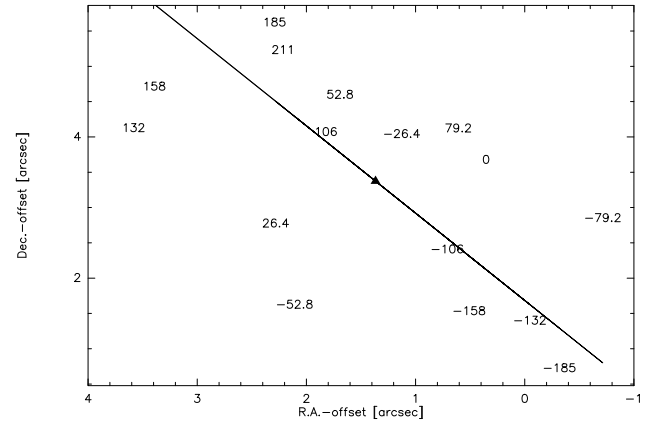
Fig. 4. Positions of Gaussian fits to the individual 10 MHz channel maps relative to the phase reference center. The triangle represents the peak of the integrated CO emission seen in Fig. 2 and coincides with the kinematical center. The line is a best fit position angle to the kinematical data.
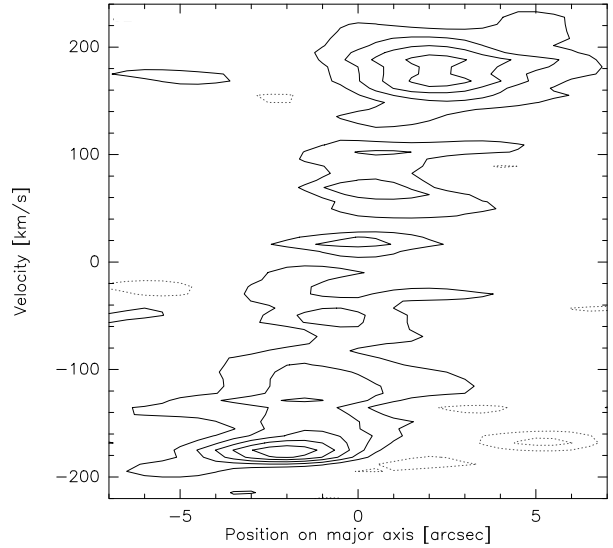

Fig. 3. a) CO(1–0) spectrum integrated over the emission region seen in Fig. 2. **b)** Single dish CO(1–0) spectrum obtained with with the IRAM 30–m telescope. **c)** Single dish CO(2–1) spectrum obtained with the IRAM 30–m telescope.

Although the extent is uncertain due to possible residual phase errors, which tend to enlarge the emission region, we will use $2''0$ (650 pc) as an 'effective radius' of the molecular gas distribution. This agrees with the average radius of a model fitted to the data (see Sect. 5.3).

4.3. The CO J=2–1/J=1–0 line intensity ratio

The extent of the CO emission region of about 4–5″ enables us to derive a size–corrected CO $J=2{-}1/J=1{-}0$ line intensity ratio. The single dish CO $J=1{-}0$ and $J=2{-}1$ spectra have integrated line intensities of $11.8\,\mathrm{K\,km\,s^{-1}}$ and $15.2\,\mathrm{K\,km\,s^{-1}}$, respectively. Convolving the Gaussian telescope HPBW of $23''$ for the CO(1–0) line and $12''$ for

Fig. 5. Position–velocity diagram along the major axis indicated in Fig. 4. The level spacing is $8\,\mathrm{mJy/beam}$. The offsets are measured relative to the position of maximum integrated emission (cf. Fig. 2). Velocities are relative to the systemic velocity.

the CO(2–1) line with a Gaussian shaped source distribution of HPBW $4''0$, we get a $J=2{-}1/J=1{-}0$ line ratio of 0.4. This value is much lower than what is expected from optically thick and thermalized CO emission and, since the source size is small compared to both telescope beams, represents a good estimate.
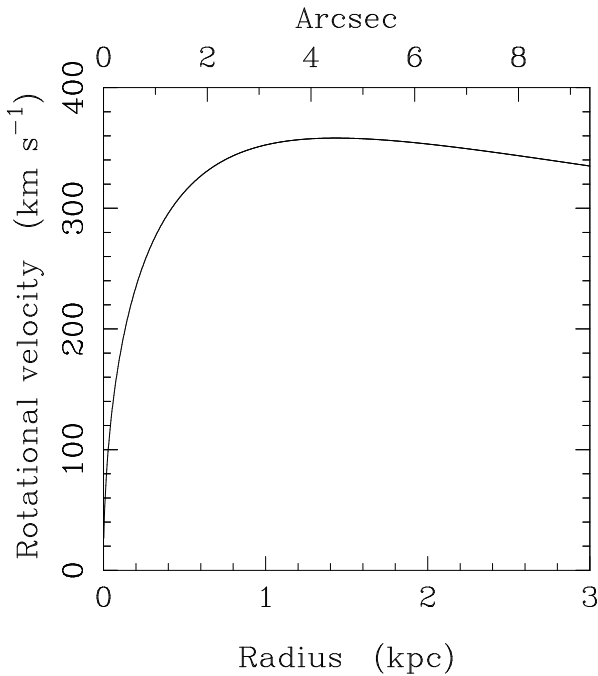
Fig. 6. The rotation curve corresponding to a spherical galaxy with an $r^{1/4}$ projected luminosity profile (Sect. 5.1). The angular scale on top corresponds to a distance of 66 Mpc.

4.4. Comparison with radio continuum

The 1.4 GHz radio continuum emission of NGC 759 has been resolved with the Very Large Array (Feretti & Giovannini 1994). Its structure is characterized by diffuse emission without a compact core. The ratio between radio and FIR fluxes is in agreement with that of star forming galaxies. A comparison of the distribution of the radio continuum emission and the molecular gas shows that the continuum emission is centered on the peak of the molecular gas distribution and that it is contained within the CO emission region (see Fig. 1 in Feretti & Giovannini 1994).

If the continuum emission at 1.4 GHz were due to free–free emission and the frequency turn–over lower than 1.4 GHz, we would expect a flux density of ~ 10 mJy at 113.5 GHz due to thermal emission in HII regions. A higher turn–over frequency would yield a higher flux density. We did not detect any continuum emission at 113.5 GHz with a 3σ limit of 3.9 mJy/beam. It is therefore likely that the continuum emission at 1.4 GHz is dominated by synchrotron radiation.

5. Dynamics and kinematics of NGC 759

5.1. A mass model

In order to interpret our CO data, we need to construct a reasonable model of the mass distribution in NGC 759. Since it is classified as an E0 galaxy, a spherical model with a light distribution following the de Vaucouleurs $r^{1/4}$ law
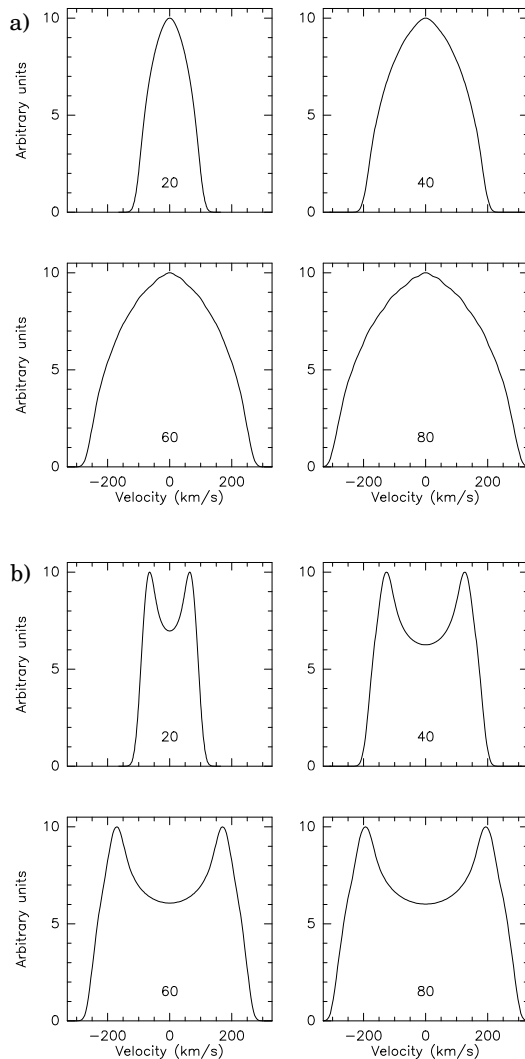

Fig. 7. Synthetic spectra of an unresolved source, derived using the formalism presented in Sect. 5.3. **a)** A filled disk and, **b)** a ring. Only the ring is compatible with the observed emission profile from NGC 759. The numbers in the spectra correspond to the inclination of the gas distribution.

is a reasonable choice. We will use the potential–density pair presented by Hernquist (1990), which closely approximates the de Vaucouleurs $r^{1/4}$ law for elliptical galaxies. This particular model has the advantage of expressing most aspects of the dynamics in an analytical form.

The mass as a function of radius is given by

$$M(r) = \frac{Mr^2}{(r+a)^2}, \tag{1}$$

where a is a parameter related to the effective radius r_{e} within which half of the luminosity is confined, $r_{\mathrm{e}} \approx 1.8153a$. M is the total mass, which we derive by first cal-
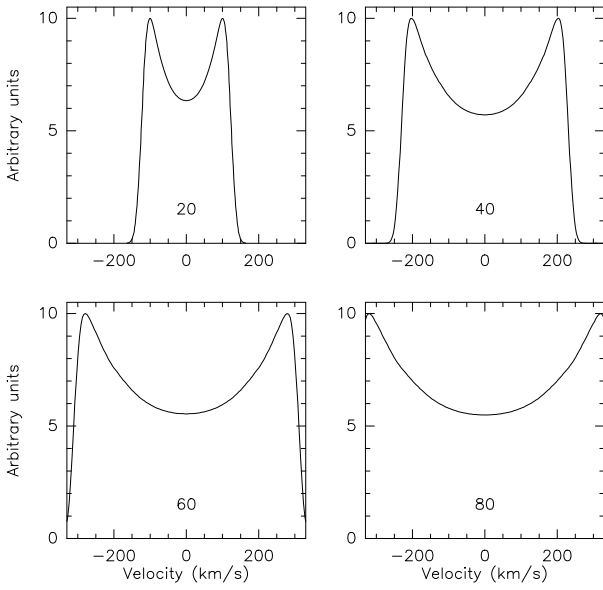
Fig. 8. Synthetic spectra obtained from the model gas distribution of NGC 759 (Sect. 5.3), viewed at different inclinations.

culating the global M/L ratio. Following Binney (1982), we have for a spherical $r^{1/4}$ galaxy,

$$\left\langle \frac{M}{L_B} \right\rangle = \frac{0.047\sigma^2}{I_e R_e}, \qquad (2)$$

where R_e is the effective radius in kpc , I_e is the surface brightness at R_e in units of $L_\odot\,pc^{-2}$ and σ is the stellar velocity dispersion in $km\,s^{-1}$. The corresponding values for NGC 759 are $R_e = 2.6\,kpc$ and $I_e = 225\,L_\odot\,pc^{-2}$ (Sandage & Perelmuter 1991). The velocity dispersion was estimated by Vigroux et al. (1989) to be $\sigma = 250\,km\,s^{-1}$. Since their value could be influenced by a higher than average velocity dispersion in the center of NGC 759, we will use $\sigma = 225\,km\,s^{-1}$as a mean value. This gives $M/L_B = 4$ in solar units and a mass of $1.4 \times 10^{11}\,M_\odot$ within a radius corresponding to R_{25} (14.5 kpc). Extrapolating to R_∞, the total mass becomes $1.7 \times 10^{11}\,M_\odot$. The circular velocity as a function of radius is

$$V_{rot} = \frac{\sqrt{GMr}}{r + a}. \qquad (3)$$

The rotation curve for NGC 759, using Eq. (3), is shown in Fig. 6. The maximum rotational velocity of $360\,km\,s^{-1}$ is reached at a galactocentric radius of 1.4 kpc. The rotational velocity at $r = 650\,pc$, the assumed extent of the molecular gas, is $330\,km\,s^{-1}$. Assuming that the molecular gas is distributed in a disk or ring–structure (see Sect. 5.3) we derive an inclination of 40° from the width of the observed emission profile.

5.2. The gas mass fraction

The total mass enclosed within a radius of 650 pc (M_{dyn}) is given by Eq. (1) as $1.7 \times 10^{10}\,M_\odot$. This constitutes 10% of the total galactic mass and results from the assumption of a constant M/L ratio and the strongly peaked luminosity distribution of elliptical galaxies. For elliptical galaxies in general, the M/L ratio tends indeed to be constant within $\sim 1.2\,R_e$ and near a value of $4\,M_\odot/L_\odot$ (Bertola et al. 1993). The M_{H_2}/M_{dyn} ratio becomes 18% within the central 650 pc, where we have included helium at a mass fraction of 1.3. As long as the mass model for NGC 759 gives the correct dynamical mass, the ratio M_{H_2}/M_{dyn} only depends on the radius of the molecular gas distribution. Whereas the gas mass fraction in the center of NGC 759 is comparable within a factor two to the gas mass fractions found in normal spiral galaxies, it falls to less than 2% when including the entire galaxy. The mass of atomic hydrogen is $< 7.4 \times 10^8\,M_\odot$ (Huchtmeier et al. 1995) and cannot greatly influence the M_{gas}/M_{dyn} ratio. Hence, NGC 759 is a gas–poor galaxy when viewed on a global scale.

The H_2 mass of NGC 759 is derived using a standard conversion factor between integrated CO emission and the column density of H_2 (cf. Wiklind et al. 1995). This ratio is unlikely to be universal, depending on excitation conditions and metallicity. For instance, if the metallicity of the molecular gas in NGC 759 is low compared to our Galaxy, we may underestimate the mass by a factor of ~ 4. This uncertainty in the molecular gas mass does not greatly influence the results discussed in this paper. The same uncertainty also applies to other galaxies with which we compare NGC 759.

5.3. The CO line profile and the molecular gas distribution

The double-horned CO profile of NGC 759 is already in itself a clue to the molecular gas distribution, ruling out too large gas concentrations in the very center. It can be shown by simple integration of the emission along the line of sight that the bulk of the CO gas should lay outside the rigid part of the rotation curve to produce the double-horned profile. For an assumed axisymmetric gas distribution of surface density $n(r)$, a typical global spectrum $dN/dv(V)$ is the sum over all radii r of

$$\frac{dN}{dv}dV = \int n(r)r\,dr\,d\theta = \int n(r)r\,dr\frac{dV}{V_{rot}(r)\sin\theta\sin i}, \qquad (4)$$

where $V_{rot}(r)$ is the rotational velocity at radius r, and i the inclination of the galaxy in the sky ($i = 0$ is face–on). Since the observed $V = V_{rot}\cos\theta\sin i$, it is straightforward to derive that in the simple but unphysical case of a constant rotational velocity V_{rot} at all radii, the double–horn profile

$$\frac{dN}{dv} \propto \left[1 - \left(\frac{V}{V_{rot}\sin i}\right)^2\right]^{-1/2}, \qquad (5)$$

results whatever the radial distribution of the surface density $n(r)$. In the opposite case of a rigid body rotation curve, and with a constant gas surface density $n(r) = n_0$ until R_{max}, where the rotation curve turns over to become flat, the spectrum becomes

$$\frac{dN}{dv} \propto \left[1 - \left(\frac{V}{V_{max} \sin i} \right)^2 \right]^{1/2}, \tag{6}$$

where V_{max} is the rotational velocity reached at R_{max}. These cases represents two extremes of rotation curves and show that a parabolic profile (large R_{max}) will transform into a double–horned when R_{max} decreases. The depth of the double-horn profile is thus a good indicator of the gas concentration with respect to the turn–over of the rotation curve. Emission profiles obtained from Eqns. (5) and (6) are shown in Fig. 7.

We have modeled in more detail the gas distribution and kinematics to better determine the constraints brought by the CO observations. We have assumed that the gas is in cylindrical rotation in a thick disk or ring, in the potential of the elliptical galaxy, as fixed in Sect. 5.1, also accounting for the potential of the gas itself. The latter is not a negligible contribution, given its high central condensation. For the disk we choose an analytical density–potential pair in the form of Toomre disks of order n=2 (cf Toomre 1964). To simulate a disk, we choose the surface density:

$$n(r) = n_0 \left(1 + \frac{r^2}{d^2} \right)^{-5/2}, \tag{7}$$

where d is the disk characteristic scale, and the corresponding rotational velocity is

$$V^2(r) = \frac{8\pi G n_0}{3d} r^2 \left(1 + \frac{r^2}{4d^2} \right) \left(1 + \frac{r^2}{d^2} \right)^{-5/2}. \tag{8}$$

For a ring, we choose the difference of two such distributions with d_1 and d_2 as characteristic scales, and with the same central surface density n_0. Since the total gas mass is fixed ($M_{H_2} = 2.4 \times 10^9 \, M_\odot$), and so is the elliptical potential, we only vary the scales d_1 and d_2. The global spectrum is then derived by a simple radial integration. A best fit with the observed spectrum is obtained for a ring constructed with scale lenghts $d_1 = 800 \, pc$ and $d_2 = 750 \, pc$, viewed at an inclination $i = 40°$ (see Fig. 8). This gives a maximum surface density of $750 \, M_\odot \, pc^{-2}$ at $r = 500 \, pc$. The surface density profile is shown in Fig. 9. Although the ring has a maximum at $500 \, pc$, the distribution is extended at galactocentric distances up to $\sim 1.5 \, kpc$ and the radius of $650 \, pc$ inferred from the interferometer data represents an average radius for the gas distribution.

Is this extended gas distribution in agreement with the barely resolved interferometric map? We have answered the question by simulating the ring with $N = 10\,000$ particles, distributed as above, with a cylindrical rotation in a

disk thickened by a $sech^2(z/z_0)$ law, with $z_0 = 200 \, pc$, and with an isotropic velocity dispersion of $30 \, km \, s^{-1}$. We then 'observed' the distribution with an inclination $i = 40°$, and an elliptical beam of $3''1 \times 2''3$. The total integrated density of the model distribution is shown in Fig. 10, and is in good agreement with the observations.
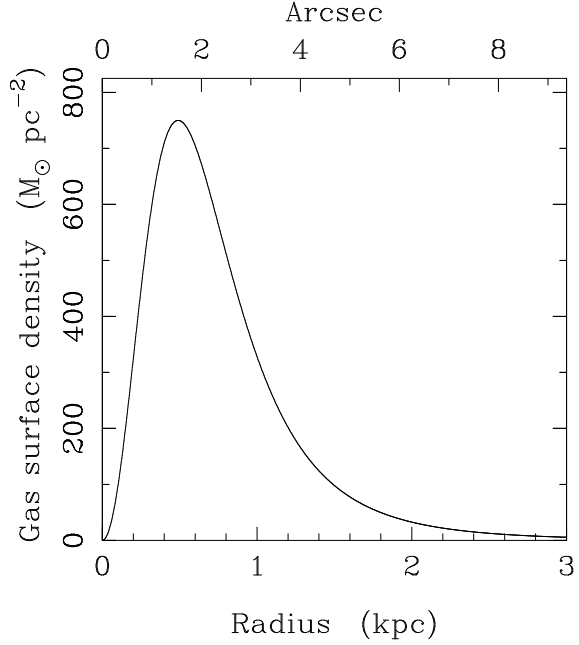

Fig. 9. The gas surface density as a function of galactocentric radius, obtained using the ring constructed from two Toomre disks (cf. Sect. 5.3).
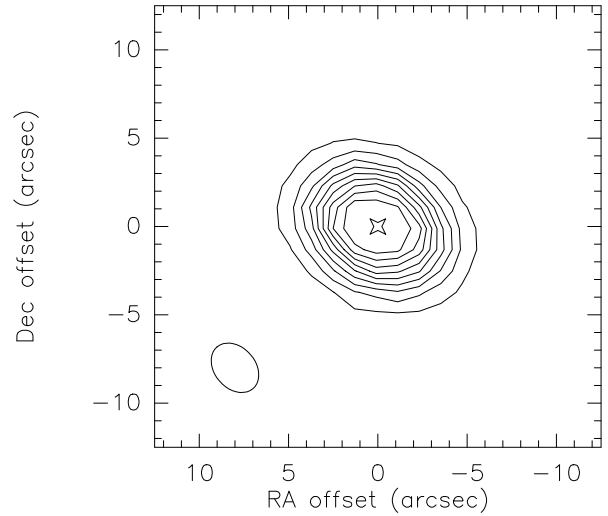

Fig. 10. A synthetic image of the ring–structure seen at an inclination of 40°, convolved with a Gaussian beam of the same HPBW size as the CLEANed beam ($3''1 \times 2''3$).

Table 3. H_2 densities and $T_B(1–0)$ for different fractional CO abundances and for CO $J=2-1/J=1-0 = 0.4$

	$X(CO)/(dV/dr)$ $(km\,s^{-1}\,pc^{-1})^{-1}$								
	10^{-6}			10^{-5}			10^{-4}		
T_k	$T_B(1–0)^{a)}$	$n(H_2)$	M_{H_2}/L_{CO}	$T_B(1–0)^{a)}$	$n(H_2)$	M_{H_2}/L_{CO}	$T_B(1–0)^{a)}$	$n(H_2)$	$M_{H_2}/L_{CO}{}^{a)}$
K	K	cm^{-3}	$M_\odot/K\,km\,s^{-1}$	K	cm^{-3}	$M_\odot/K\,km\,s^{-1}$	K	cm^{-3}	$M_\odot/K\,km\,s^{-1}$
10	2.8	1144	25	5.3	464	9	4.2	180	7
20	1.3	422	33	3.2	216	10	4.0	<100	<5
30	0.9	276	39	2.6	153	10	—	—	—
40	0.7	210	43	2.1	121	11	—	—	—
60	0.6	152	52	—	—	—	—	—	—

a) T_B is the excess brightness temperature above the microwave background.

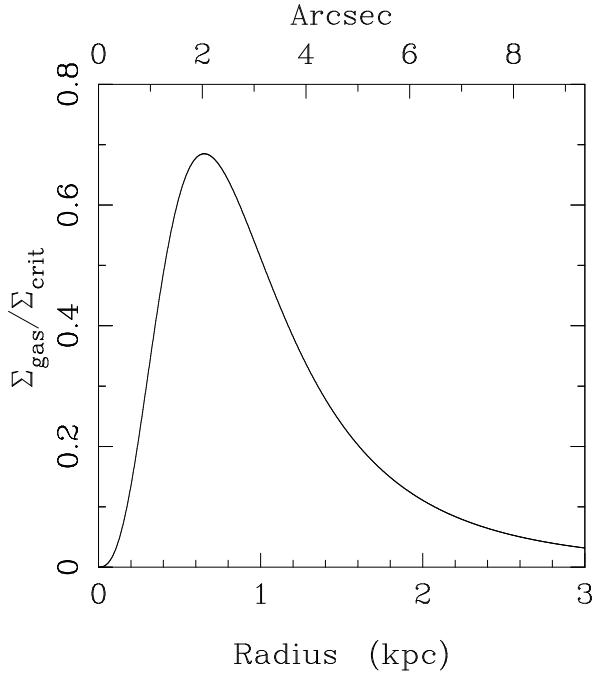b) $M_{H_2}/L_{CO} = 2.1\sqrt{n(H_2)}/T_B(1-0)$ (cf. Radford et al. 1991).

Fig. 11. The ratio of the molecular gas surface density Σ_{gas} (including helium at a mass fraction of 1.3) and the critical gas surface density Σ_{crit}, as a function of galactocentric radius for a galaxy described by the mass model presented in Sect. 5.1.

6. Discussion

6.1. Is NGC 759 a starburst elliptical?

Apart from the mere presence of molecular gas, there are three facts which suggest that massive star formation is taking place in the inner 650 pc of NGC 759: *(i)* optical emission lines from HII regions, *(ii)* diffuse radio continuum emission and *(iii)* FIR emission which most likely comes from dust heated by massive stars. With a Salpeter initial mass function, the inferred star formation rate (SFR) is $\sim 7\,M_\odot\,yr^{-1}$ (Table 1).

How does the molecular data fit into the picture of NGC 759 as an actively star forming elliptical galaxy? Below we discuss the molecular properties in more detail in view of its implications for the star formation activity in NGC 759.

6.2. The molecular gas surface density and Σ_{crit}

Kennicutt (1989) has argued for the existence of massive star formation activity in spiral galaxies only when the gas surface density exceeds a critical value, for which the gaseous disk is expected to become unstable to large scale density perturbations. Using the Toomre (1964) formulation, the critical surface density can be expressed as:

$$\Sigma_{crit} = \alpha\frac{\kappa c}{\pi G}, \tag{9}$$

where α is a constant of order unity (0.7 for spiral galaxies), κ is the epicyclic frequency, c is the gas velocity dispersion and G the gravitational constant. Using the rotation curve corresponding to the mass model presented in Sect. 5.1, the critical gas surface density becomes

$$\Sigma_{crit} \approx 1.6\frac{V_{rot}}{r}\sqrt{3 - \frac{2r}{r+0.55r_e}}\ M_\odot\,pc^{-2}, \tag{10}$$

where r is the galactocentric distance expressed in kpc, V_{rot} is the rotational velocity in $km\,s^{-1}$, and we have assumed a gas velocity dispersion of $30\,km\,s^{-1}$. The ratio of the molecular gas surface density obtained from the model distribution presented in Sect. 5.3 and the Σ_{crit} derived using Eq. (10) is shown in Fig. 11. Due to the rapid increase of Σ_{crit} with decreasing radius, the ratio is everywhere less than one. Despite the high molecular gas surface density we do not expect the gas to be highly susceptible to large scale density perturbations. The ratio is, however, of order unity around the peak of the molecular ring, and this

allows gravitational instabilities to develop on the same scale as in the disk of normal spiral galaxies. The maximum of $\Sigma_{\mathrm{gas}}/\Sigma_{\mathrm{crit}}$ falls at a slightly larger galactocentric distance than the peak of the molecular ring. A thin ring of HII regions should therefore be visible in narrow band $H\alpha$ images at a distance of $\sim 2\rlap{.}''0$ from the nucleus of NGC 759.

6.3. $\Sigma_{\mathrm{H_2}}$ and the $L_{\mathrm{FIR}}/M_{\mathrm{H_2}}$ ratio

The molecular gas surface density of $750\,\mathrm{M_\odot\,pc^{-2}}$ found for NGC 759 is high when compared with the Galactic molecular ring ($12\,\mathrm{M_\odot\,pc^{-2}}$) and the Galactic center region ($200 - 300\,\mathrm{M_\odot\,pc^{-2}}$), but it is a factor $2 - 3$ smaller than the surface density obtained by assuming a constant surface density disk truncated at a radius $650\,\mathrm{pc}$. In the latter case NGC 759 would have a gas surface density similar to those of ultraluminous FIR galaxies (cf. Scoville et al. 1991). The difference comes from the larger extension of the CO distribution at low surface density (out to $1.5\,\mathrm{kpc}$) in the modelled ring distribution (see Sect. 5.3).

In Fig. 12 we compare the $L_{\mathrm{FIR}}/M_{\mathrm{H_2}}$ ratio vs. $\Sigma_{\mathrm{H_2}}$ for ultraluminous FIR galaxies and NGC 759, with $\Sigma_{\mathrm{H_2}}$ derived assuming a truncated gas disk and using the virial theorem. NGC 759 has an $L_{\mathrm{FIR}}/M_{\mathrm{H_2}}$ ratio of $4.7\,\mathrm{L_\odot/M_\odot}$, which is much smaller than for ultraluminous FIR galaxies who typically have ratios in excess of $40\,\mathrm{L_\odot/M_\odot}$. In fact, the $L_{\mathrm{FIR}}/M_{\mathrm{H_2}}$ ratio of NGC 759 is only half the average value for normal IRAS selected spiral galaxies (cf. Young et al. 1989). The large $\Sigma_{\mathrm{H_2}}$ of NGC 759 and the low $L_{\mathrm{FIR}}/M_{\mathrm{H_2}}$ ratio suggests that NGC 759 is underluminous in L_{FIR} with respect to its $\mathrm{H_2}$ mass as compared to ultraluminous FIR galaxies. This could be caused by a lack of massive stars heating the dust in NGC 759, suggesting a low star formation efficiency, or the presence of an extra heating source of the dust in ultraluminous FIR galaxies, possibly an AGN. If the metallicity of the molecular gas in NGC 759 should be very low, which it could be if the gas was accreted from a dwarf galaxy, the $\mathrm{H_2}$ mass would be underestimated, enhancing the difference between NGC 759 and the ultraluminous FIR galaxies.

6.4. Subthermal excitation of the CO emission

A CO $J=2-1/J=1-0$ line ratio as low as 0.4 (Sect. 4.3) is rarely encountered in molecular clouds, neither in our Galaxy nor in external spiral galaxies (Braine & Combes 1992). The low ratio implies a subthermal excitation of the J= 2 level and is usually interpreted as cold and/or diffuse molecular gas.

Table 3 summarizes large velocity gradient calculations for a CO $J=2-1/J=1-0$ ratio of 0.4. The calculations are taken from Castets et al. (1990) and give for three different fractional CO abundances per velocity interval, $X(\mathrm{CO})/(dV/dr)\,(\mathrm{km\,s^{-1}\,pc^{-1}})^{-1}$, the brightness temperature T_{B}, the $\mathrm{H_2}$ density and the ratio $M_{\mathrm{H_2}}/L_{\mathrm{CO}}$. $X(\mathrm{CO})$

is equal to $n(\mathrm{CO})/n(\mathrm{H_2})$. A small fractional CO abundance can be interpreted as a low metallicity gas and a large abundance as a high metallicity gas. The $M_{\mathrm{H_2}}/L_{\mathrm{CO}}$ ratio is derived in the same way as in Radford et al. (1991). A value of $4.5\,\mathrm{M_\odot/L_\odot}$ corresponds to the standard $N_{\mathrm{H_2}}/I_{\mathrm{CO}}$ conversion ratio.

A fractional CO abundance lower than $10^{-6}\,(\mathrm{km\,s^{-1}\,pc^{-1}})^{-1}$ can be excluded on grounds of a very low brightness temperature and an $M_{\mathrm{H_2}}/L_{\mathrm{CO}}$ ratio $\sim 10^3\,\mathrm{M_\odot/L_\odot}$. In the case of a small fractional CO abundance we underestimate the molecular mass by a factor 5–10, whereas a high fractional abundance gives the correct mass to within a factor of 2. In the simple hypothesis of a homogeneous one–component medium, under the LVG approximation, two extreme physical conditions are possible for the molecular gas: either cold and dense ($T_{\mathrm{k}} \approx 10\,\mathrm{K}$, $n(\mathrm{H_2}) \gtrsim 10^3\,\mathrm{cm^{-3}}$) or warm and diffuse ($T_{\mathrm{k}} \approx 40\,\mathrm{K}$, $n(\mathrm{H_2}) \approx 10^2\,\mathrm{cm^{-3}}$). A more realistic solution might be a multi–medium composed of dense clumps embedded in a diffuse component, where the CO emission is dominated by the diffuse component while most of the mass is contained in the dense clumps. This can be seen from the higher $M_{\mathrm{H_2}}/L_{\mathrm{FIR}}$ ratio of the cold and dense component compared to the diffuse gas (see Table 3).

6.5. Comparing with a bonafide merger: NGC 7252

A good example of an advanced merger is NGC 7252, which shows evidence of a recent starburst in its center (cf. Schweizer 1982). Although the merger initially consisted of two disk galaxies, the overall light distribution now follows the $r^{1/4}$ law (Schweizer 1982, Stanford & Bushouse 1991).

Dupraz et al. (1990) observed NGC 7252 in the CO $J=1-0$ and $J=2-1$ lines with a single dish telescope (SEST), and Wang et al. (1992) observed it with the Owens Valley interferometer, achieving a resolution of $3\rlap{.}''8 \times 2\rlap{.}''1$ ($1.1 \times 0.6\,\mathrm{kpc}$, assuming a distance of $63\,\mathrm{Mpc}$). The molecular gas distribution in NGC 7252 has a striking resemblance to that of NGC 759. The CO profiles from the single dish and the interferometer are double–horned, and the inclination of the gas appears to be around $40°$. At least 72% of the CO(1–0) emission in NGC 7252 comes from within a radius of $1.5\,\mathrm{kpc}$. The CO $J=2-1/J=1-0$ ratio, corrected for the size of the emission region, is $0.4 - 0.6$ (depending on how much of the CO(2–1) emission that is extended). The molecular gas surface density of NGC 7252 is similar to NGC 759, when calculated in the simple way discussed in Sect. 5.2. However, while the dust temperatures are comparable, the $L_{\mathrm{FIR}}/M_{\mathrm{H_2}}$ ratio of NGC 7252 is a factor 3 higher than in NGC 759

Since the projected light distribution of NGC 7252 closely follows the $r^{1/4}$ law, it is appropriate to use a mass model similar to the one we used for NGC 759 (Sect. 5.1). From the light profile presented by Stanford & Bushouse (1991) we derive an effective radius r_{e} of $10\rlap{.}''8$ ($3.3\,\mathrm{kpc}$).

If we express the total mass of NGC 7252 as a function of the mass–to–light ratio,

$$M_{\text{tot}} = \left\langle \frac{M}{L_{\text{B}}} \right\rangle L_{\text{B}}, \qquad (11)$$

and use Eq. (1) and (2), we get the following expressions for the mass within radius $r = 1.5\,\text{kpc}$ and the corresponding rotational velocity,

$$M(r) = 9.4 \times 10^9 \left\langle \frac{M}{L_{\text{B}}} \right\rangle \, \text{M}_\odot, \qquad (12)$$

$$V(r) = 166 \sqrt{\left\langle \frac{M}{L_{\text{B}}} \right\rangle} \, \text{km s}^{-1}. \qquad (13)$$

The H_2 mass within a radius of $1.5\,\text{kpc}$ is $3 \times 10^9\,\text{M}_\odot$ (Wang et al. 1992), giving a M_{H_2}/M_{dyn} ratio of $0.3 \langle M/L_{\text{B}} \rangle^{-1}$. The mass–to–light ratio must be at least 3 to give the observed velocity width ($i = 90°$). This gives a molecular gas mass fraction of $\lesssim 10\%$ in the inner region of NGC 7252. This is considerably smaller than the 45% derived by Wang et al. (1992). If the inclination is in the range $40° - 50°$, as implied by the interferometer map, the mass–to–light ratio is $5 - 7$, further diminishing the molecular gas mass fraction.

Apart from the L_{FIR}/M_{H_2} ratio, the advanced merger NGC 7252 and the elliptical NGC 759 show striking similarities in their molecular gas properties.

The very high gas mass fractions found in the central regions of ultraluminous FIR galaxies (cf. Scoville et al. 1991), including NGC 7252, have been obtained from a dynamical mass derived using the virial theorem. This is applicable to disk systems with a small central mass concentration compared to elliptical galaxies. However, most of these ultraluminous FIR galaxies are mergers, and presumably have a light distribution following the $r^{1/4}$ law. Hence, it would be appropriate to use a more concentrated mass model such as that described by Hernquist (1990). This would decrease the central gas mass fractions in ultraluminous FIR galaxies by a factor $3 - 10$.

7. Summary and conclusions

NGC 759 is an elliptical galaxy which contains $2.4 \times 10^9\,\text{M}_\odot$ of molecular gas, most of it confined to a circumnuclear ring with an average radius of $\sim 650\,\text{pc}$. The average molecular gas surface density in the center region of NGC 759 is $750\,\text{M}_\odot\,\text{pc}^{-2}$. Although this value is high, it is always less than the critical gas surface density for large scale gravitational instabilities. The low CO $J=2-1/J=1-0$ line ratio of 0.4, is consistent with a molecular gas consisting of cold and dense clumps ($T_{\text{k}} \approx 10\,\text{K}$, $n(H_2) \gtrsim 10^3\,\text{cm}^{-3}$) embedded in a warm and diffuse molecular gas ($T_{\text{k}} \approx 40\,\text{K}$, $n(H_2) \approx 10^2\,\text{cm}^{-3}$). The dense component contains most of the molecular gas mass,
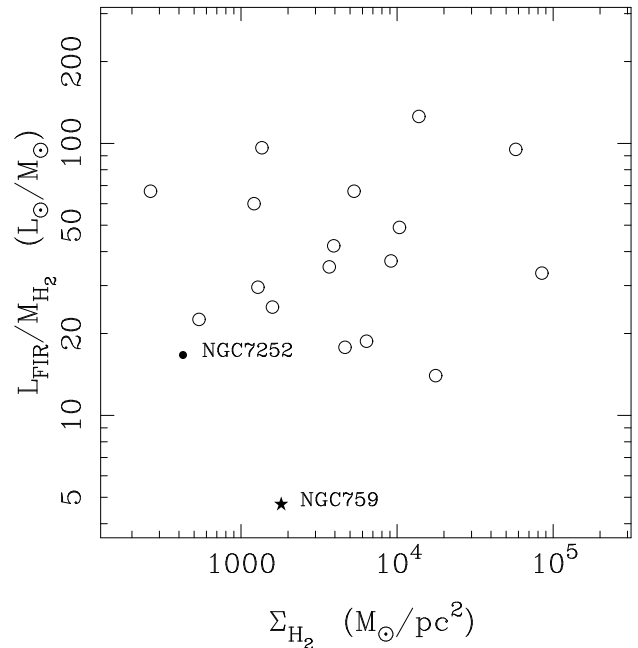

Fig. 12. The L_{FIR}/M_{H_2} ratio as a function of the average nuclear molecular gas surface density for ultraluminous far–infrared galaxies (open circles), NGC 7252 (filled circle) and NGC 759 (star). The gas surface density has been derived in the same manner for all galaxies; using a truncated gas disk and the virial theorem.

while the diffuse gas dominates the emission. Finally, when compared with galaxies of similar gas surface densities, NGC 759 appears to be underluminous in L_{FIR} with respect to its molecular gas mass by a factor $3 - 10$.

In a quiet environment, molecular gas condenses into a very clumpy structure with local high densities and a low volume filling factor, resulting in a low average gas surface density. Intense star formation partially destroys the clumpy structure and the fraction of diffuse molecular gas is considerably enhanced. Consequently the filling factor and the average surface density will also increase. Although the kinetic temperature increases due to these processes, the CO excitation temperature can become quite low due to subthermal excitation caused by the low volume density of H_2.

This scenario, which seems to be applicable to NGC 759, implies that star formation is ongoing and has been so long enough to influence the molecular gas properties in the circumnuclear ring. The low L_{FIR}/M_{H_2} ratio could have its explanation in the lack of an additional heating source for the dust in the form of an AGN.

The high concentration of molecular gas in the center of NGC 759, the lack of atomic gas and the relatively modest amount of star forming activity is reminiscent of the conditions found in the merger NGC 7252. The main difference being that while NGC 7252 exhibits gas–rich tidal

tails and a high star formation efficiency, NGC 759 shows no sign of gravitationally induced disturbances and has a low star formation efficiency.

The cluster A262 contains a high fraction of spiral galaxies (75%). The spirals are less centrally concentrated and have a higher line–of–sight velocity dispersion then the ellipticals (Moss & Dickens 1977). NGC 759 is situated in outer parts of A262, at a projected distance of 1.4 Mpc from the cluster center. Could NGC 759 represent a very late stage in the merging of two disk galaxies? The fate of the gaseous component in the merging of two gas rich galaxies is two–fold: a major part of the gas looses angular momentum quickly and falls towards the center while the merging process is on–going. If this gas component is capable of forming stars, it can produce the high stellar phase–space density characteristic for elliptical galaxies. The other part of the gas is ejected into tidal arms, which remain bound to the system (Hernquist & Spergel 1992; Hibbard & Mihos 1995). This gas will fall back to the galaxy at later times. If elliptical galaxies are formed through the merging of two gas rich disk galaxies, an important question is: where are the galaxies which are in between the final product, an inert and gas–free elliptical galaxy, and those which still show signs of the merging process, such as NGC 7252. This question was first raised by I. King and has been named the 'King Gap'. Galaxies in the 'King Gap' should look like proverbial elliptical but still retain some signatures of the merging process. These signatures can be:

- Gas and dust components as well as an intermediate aged stellar population.
- Optical fine structure in the form of faint shells, ripples and boxy isophotes (cf. Schweizer & Seitzer 1992).
- Kinematically distinct sub–systems (cf. Surma & Bender 1995).
- Gas in the outer part of the tidal arms require very long time scales to return to the galaxy. Hence, one would expect the presence of low HI column density at large galactocentric distances (cf. Hibbard & Mihos 1995).

NGC 759 does show unusual gas properties for an elliptical galaxy and if it represents a galaxy in the 'King Gap', one or more of the additional signatures should be found in a more extended study.

References

Aaronson M., Huchra J., Mould J., Schechter P.L., Tully R.B., 1982, ApJ 258, 64

Balcells M., Stanford S.A., 1990, ApJ 362, 443

Bertola F., Bettoni D., 1988, ApJ 329, 102

Bertola F.,Pizzella A., Persic M., Salucci P., 1993, ApJ 416, L45

Binney J.J., 1982, ARA&A 20, 399

Braine J., Combes F., 1992, A&A 264, 433

Braine J., Dupraz C., 1994, A&A 283, 407

Caldwell N., 1984, PASP 96, 287

Castets A., Duvert G., Dutrey A., et al., 1990, A&A 234, 469

de Vaucouleurs G., de Vaucouleurs A., Corwin H.G., et al., 1991, Third Reference Catalogue of Bright Galaxies, Springer–Verlag New York Inc. (RC3)

Djorgovski S., Davis M., 1987, ApJ 313, 59

Dupraz C., Casoli F., Combes F., Kazès I., 1990, A&A 228, L5

Ebneter K., Balick B., 1985, AJ 90, 183

Fabbiano G., 1990, ARA&A 27, 87

Faber S.M., Gallagher J.S., 1976, ApJ 204, 365

Feretti L., Giovannini G., 1994, A&A 281, 375

Franx M., Illingworth G., 1988, ApJ 327, L55

Guilloteau S., Delannoy J., Downes D., et al., 1992, A&A 262, 624

Guzmán R., Lucey J.R., Bower R.G., 1993, in ESO/EPIC Workshop on Structure, Dynamics and Chemical Evolution of Elliptical Galaxies, eds. I.J. Danziger, W.W. Zeilinger, K. Kjär, ESO Conference and Workshop Proc. No. 45, p. 19

Hernquist L., 1990, ApJ 356, 359

Hernquist L.E., Barnes J.E., 1991, Nature 354, 210

Hernquist L.E., Spergel D.N., 1992, ApJ 399, L117

Hibbard J.E., Mihos J.C., 1995, AJ 110, 140

Huchtmeier W.K., Sage L.S., Henkel C., 1995, A&A 300, 675

Jones C., Forman W., 1984, ApJ 276, 38

Jura M., Kim D.W., Knapp G.R., Guathakurta P., 1987, ApJ 312, L11

Kennicutt R.C., 1989, ApJ 344, 685

Knapp G.R., Guhathakurta P., Kim D.–W., Jura M., 1989, ApJS 70, 329

Knapp G.R., Turner E.L., Cunniffe P.E., 1985, AJ 90, 454

Lees J.F., Knapp G.R., Rupen M.P., Phillips T.G., 1991, ApJ 379, 177

Moss C., Dickens R.J., 1977, MNRAS 178, 701

Phillips M.M., Jenkins C.R., Dopita M.A., Sadler E.M., Binette L., 1986, AJ 91, 1062

Radford S.J.E., Solomon P.M., Downes D., 1991, ApJ 368, L15

Rix H.–W., White S.D.M., 1992, MNRAS 254, 389

Sandage A., Perelmuter J.–M., 1991, ApJ 370, 455

Schweizer F., 1982, ApJ 252, 455

Schweizer F., Seitzer P., 1992, AJ 104, 3

Scoville N.Z., Sargent A.I., Sanders D.B., Soifer B.T., 1991, ApJ 366, L5

Stanford S.A., Bushouse H., 1991, ApJ 371, 92

Surma P., Bender R., 1995, A&A 298, 405

Toomre A., 1964, ApJ 139, 1217

Vigroux L., Boulade O., Rose J., 1989, AJ 98, 2044

Wang Z., Schweizer F., Scoville N.Z., 1992, ApJ 396, 510

Wiklind T., Combes F., Henkel C., 1995, A&A 297, 643

Young J.S, Shuding X., Kenney J.D.P., Rice W.L., 1989, ApJS 70, 699